NJC

High surface area of carbonaceous Cr2GaC composite microspheres synthesized by sol–gel chemistry

SCHOLARONE™
Manuscripts

ARTICLE

High surface area of carbonaceous Cr$_2$GaC composite micro-spheres synthesized by sol-gel chemistry

Jordan Sinclair[a], Jan P. Siebert[a], Matt Flores[a], David Ciota[a], Dong-Kyun Seo[a], *Christina S. Birkel[a,b]

[a.] School of Molecular Sciences, Arizona State University, Tempe AZ-85282, USA. Email: Christina.Birkel@asu.edu
[b.] Eduard-Zintl-Institute, Technische Universität Darmstadt, Alarich-Weiss-Straße 12, 64287 Darmstadt, Germany

Corresponding author: Christina S. Birkel, christina.birkel@asu.edu

MAX phases are wildly renowned for incorporating metallic and ceramic properties into a single compound but lack high degrees of porosity. Using a sol-gel chemistry technique, known as a Polymer Type II complex method, more flexibility to the shape, morphology, microstructure, and porosity is achieved while simultaneously synthesizing MAX phase. This sol-gel chemistry techique demonstrates a signficant departure from traditional solid state synthetic methods. Temperature profiles in this study allowed discussions of the influence of furnace and microwave heating on the resulting products. The carbonaceous Cr$_2$GaC spheres were identified to exhibit Type IV isotherm behavior and a hysteresis type of H2(a). Micropore surface areas ranged from 220-416 m^2/g and the maximum BET specific surface area received was 616 m^2/g,.

Introduction

Ternary carbides and (carbo)nitrides that belong to the family of MAX phases have been held in high regard since their discovery in 1960[1] and eventual resurgence in 1996.[2] MAX phases crystallizing in the hexagonal space group $P6_3/mmc$ are described by the general formula M$_{n+1}$AX$_n$ (n = 1, 2, 3, 4) where M = early-to-mid-transition metals, A = main group elements, mostly from groups 13 and 14, and X = carbon and/or nitrogen. Largely known for their ability to couple ceramic and metallic properties into a singular compound, they are currently commercially used as high-performance coatings, and nuclear power plant claddings.[3–5] With well over 150 different compounds of these materials to date, the main focus currently resides on Ti-Al-C based systems.[6–8] Unsurprisingly, this has come as a result of the complementary interest in the 2D MXenes, which MAX phases are a precursor phase for. [9,10]

Apart from being used as coatings to make devices more resistive against extreme conditions,[5,11,12] MAX phases have found no wide-spread commercial use. Due to this they have been largely relegated to theoretical speculation for potential uses. Some of these uses include incorporation into high efficiency engines, directly into nuclear reactors, and indirectly in the production of asymmetric supercapacitors.[4,13] Even more, MAX phases and their 2D siblings, MXene, have also shown potential in the realm of catalysis and in gas adsorption. [14–21] Most importantly, as it relates to this work, is the inclusion of MAX phases into composite materials. Whether this is realized by means of ex situ or wet chemical processing, many works exist detailing the possibilities to utilize these types of compounds in a variety of different applications.[22–24]

Following these ideas, it is well known MAX phases innately possess low surface areas.[11,25] Their incorporation into material composites that are microporous in nature can unlock enhanced hybrid properties. Solid state heating techniques, unfortunately, do not possess the capabilities to achieve this goal in a singular step. MAX phase material will need to be made separately via solid state heat treatments with elemental reagents and then additionally added to porous material.[22–24] Moreover, the level of atomistic homogeneity is not equivalent to what can be obtained using methodologies like sol-gel chemistry.[26] Recently, a method known as the amorphous metal complex method has become a viable synthesis strategy for MAX phase synthesis and yield optimization. Phases such as Cr$_2$GaC, Cr$_2$GeC, V$_2$GeC, V$_2$GaC, V$_2$GaC$_{1-x}$N$_x$, and V$_2$PC have all been produced utilizing this technique.[27–31] Shape processability using this approach is limited though. Remedying this required a pivot toward another sol gel

technique known as the Polymer Type II complex method.[26] Here natural product derived biopolymers such as Chitosan are taken advantage of to complex metal ions dispersed into a gel matrix.[32] Shape augmentation into wires, spheres, films, etc. all become possible.[32,33] Chitosan innately being porous makes it a great candidate for pore composite templating with the synthesized MAX phase. With this, we aim to hybridize metallic/ceramic properties, with high degrees of porosity, and all through a single synthetic heat treatment step. BET surface analysis and sorption measurements of the carbonaceous composite microspheres are performed to pave the way to suitable applications.

Experimental

Materials and Methods

Materials

Chromium (III) Nitrate Nonhydrate (Acros Organics, 99.9%), Gallium Nitrate Hydrate (Alfa Aesar, 99.9%), and Chitosan (Medium Molecular Weight 190,000-310000 KDa, Sigma Aldrich) were all used with no processing applied to them.

Synthesis of Cr_2GaC Composite Spheres

In a typical synthesis, 2.000 g of $Cr(NO_3)_3\cdot9H_2O$ (2 eq, 5 mmol) and 0.7375 g of $Ga(NO_3)_3\cdot H_2O$ (1 eq, 2.69 mmol) were weighed and added to a beaker containing 10 mL of water and vigorously stirred using a magnetic stir bar. In another beaker, 0.6 g of Medium Molecular Weight Chitosan, 1 mL of Acetic Acid, and 4 mL of the previously made Cr:Ga metal solution were mixed thoroughly in 20 mL water. Chitosan was chosen as carbon source for its inherent properties of acting as a proton absorber/chelating agent[32] , being very porous in nature, and most importantly its insolubility in basic solutions. Therefore, performing sol-gel chemistry, where metal ions are mixed intimately with this natural biopolymer, allows for it to act as a template for significant levels of porosity. Stirring continued for 20-30 minutes to ensure complete homogenization of the mixture. Using a blunt dispensing tip and syringe (CML supply), the Cr:Ga chitosan metal solution was added to a 1M NH_4OH solution dropwise. The metal chitosan macrospheres (1.60 - 2.98 mm in length) were precipitated in the dilute NH_4OH solution, filtered, and then transported to a watch glass. The macrospheres were left overnight at 35 °C to evaporate excess moisture and ammonia. The dried spheres were then subsequently heat treated by two different methods: Conventional furnace as well as microwave heating. For the conventional method, the dried spheres were loaded into an alumina boat and transferred to a tube furnace (Carbolite). The

system environment was purged for 30 minutes with UHP Argon. A heating profile of ramping 2 °C per minute to 1050 °C, dwell for 2 hours at 1050 °C, and cooling to room temperature was applied. For the non-conventional heat treatment, dried spheres were transported down an alumina tube. This alumina tube was then inserted into a fused silica ampoule. 7.000 g of susceptor (Activated Charcoal 12-20 mesh, granular) were added to a high alumina crucible (Coors). The fused silica ampoule and sample were positioned in the middle/toward the bottom of the susceptor to ensure uniform heating. The system chamber of the microwave reactor (CEM Mars) was flushed with the sample using UHP Argon for 20-30 mins. A heating profile of 700 W (approximately 700-750 °C) for 20 mins was applied to the sample. The resulting microspheres after both the furnace and microwave treatment were recovered for further analysis. All microspheres across all gauge sizes were analyzed in four different states (wet, dry, furnace heat treated, and microwave heat treated). In the wet state when the spheres were precipitated, they were positioned onto a petri dish and placed directly under a microscope. Using LAS EZ software, a digital snapshot of about 100 spheres was taken with a scale bar. Following this, the software Image J was used to set scale and draw line segments across at least 50 spheres. The sphere diameters were averaged automatically using the measure and summarize function. To ensure the average from Image J was correct, the spread of data was also averaged in Excel. This entire procedure was repeated across the remaining processing steps and then repeated across all gauge sizes.

Materials Characterization

Powder X-ray Diffraction/ Rietveld Refinements

All samples were ground with an agate mortar pestle and placed on top of a flat cylindrical Si low background stage. The X-ray diffraction data were recorded using a Bruker D2 Phaser (2nd Generation) powder X-ray Diffractometer that utilizes Ni-filtered Cu Kα radiation (λ = 1.5406) at room temperature. The 2θ ranges extended from 10°–90° with a step size of 0.05°. The experimental patterns generated were then subsequently matched with theoretical profiles for the most accurate phase determination. Analysis of the percentages of existing phases in bulk samples were carried out by Rietveld refinement with the assistance of Topas.[34]

BET Measurements Surface Analysis Theory

Surface area analysis of the Cr_2GaC-based spheres was performed on a Micromeritics ASAP 2020 Surface Area and Porosity Analyzer with nitrogen as the adsorbate at 77 K. This was performed for samples generated from furnace synthesis with selective gauge sizes ranging from 17-30

gauge (1.4 - 0.31 mm). Similarly, microwave synthesis samples were measured also with the same selective size ranges (17-30 gauge, 1.4 - 0.31 mm). The sample weight for each BET was chosen to be around 100 mg. All samples were degassed for approximately 10 hours at 200 °C with residual pressure less than 50 µmHg. The surface areas were determined using the Brunauer-Emmett-Teller (BET) model.[35] Micropore and external surface areas were determined through the t-plot method. Pore size distributions were generated using the Barret-Joyner-Halenda (BJH) method.[35]

SEM/EDS

Analysis of the microstructure was performed using an Auriga-Zeiss FIB SEM. The composition of samples was determined utilizing an Oxford Instruments SDD detector (Ultim MAX). A standard aluminum stage holder was covered with carbon tape to fasten 10-20 spheres to the holder surface. The beam current was set at a 20 keV accelerating potential primarily for the EDS that was conducted. Multiple sites of the bulk samples were analyzed at varying magnifications (ranging from 1K-70K magnification).

TEM and HR-TEM

Cr_2GaC sphere powder samples were dispersed in ethanol and sonicated for 30 min, and the resulting solution was drop cast onto a lacey carbon TEM grid. Samples were analyzed using the monochromated environmental FEI Titan ETEM aberration-corrected TEM with a Schottky field emission gun. A 300 kV acceleration voltage was used to collect micrographs, Gatan software was used to process the data, and Image J was used to format the imaging further.

Results and Discussion

Table 1. Size diameters of the MAX microspheres at various different states of the sol-gel synthesis methodology.

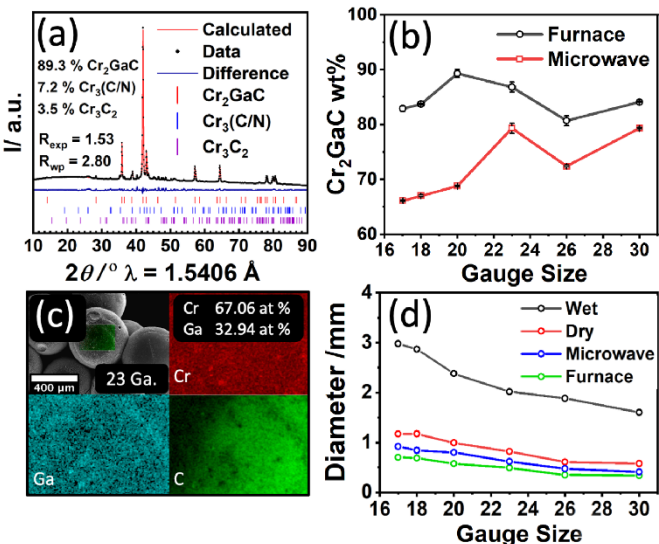| Gauge Size mm/ga	Wet (mm)	Dry (mm)	Microwave (mm)	Furnace (mm)
1.4/17	2.98	1.17	0.92	0.70
1.27/18	2.87	1.18	0.84	0.69
0.91/20	2.38	0.99	0.80	0.58
0.64/23	2.02	0.82	0.62	0.49
0.46/26	1.88	0.61	0.48	0.35
0.31/30	1.60	0.58	0.41	0.34

Figure 1. (a) Exemplary X-ray powder diffraction data including Rietveld refinement of Composite-Cr_2GaC microspheres, (b) Cr_2GaC wt% comparison relative to different gauge sizes and heating methods, (c) exemplary elemental analysis (EDS) of Composite microspheres (furnace treatment, 23-gauge needle), (d) microsphere diameter in dependence of the gauge size as obtained.

Following our synthesis protocol reported in [32], all composite spheres were shape processed by using needle gauge sizes ranging from 0.31 mm – 1.4 mm (17–30-gauge size). All averaged diameters of the composite spheres are reported in Table 1. A reliable shrinkage of the microspheres in all states is depicted in Figure 1, panel (d). Varying the gauge size, it was assumed that testing the BET specific surface areas (SSAs) would influence the gas sorption capabilities. Rietveld analysis of furnace heat treated/annealed microspheres produced with a 20-gauge needle (Figure 1 (a)) shows an 89 % yield of the target Cr_2GaC MAX phase. Due to the use of nitrate salt precursors ($Cr(NO_3)_3$ and $Ga(NO_3)_3$) it is plausible for nitrogen-based side phases to crystallize with roughly 8 wt%. Across all gauge sizes and heat treatments Cr_2GaC wt% yield ranges from 66-89%. SEM/EDS analyses (Figure 1 (c)) confirm a 2:1 ratio of Cr to Ga in 23 ga microspheres and all other gauge sizes when pyrolyzed in the furnace, Figures S14-21. Microwave composite spheres exhibit a non-stochiometric ratio of Cr:Ga because of Ga tendency to bleed/bead up from the material. (See Figure S14-S21 in SI for more information on SEM/EDS of furnace and microwave samples). Although, since the focus is on the assessing the

gas sorption capabilities of the composite spheres, we place more emphasis on that.

In Figure 2, all the nitrogen sorption isotherms of the furnace-annealed samples show similar behaviors with a gradual but significant uptake in the low P/P_o region, indicating appreciable presence of micropores. The estimated BET specific surface areas (SSAs) range from 396-616 m^2/g^{-1} on the low and high end, respectively,
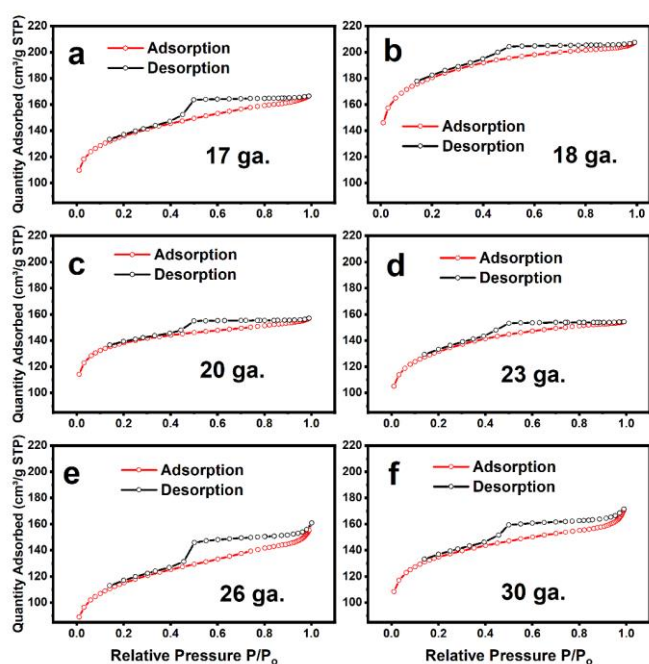

Figure 2. Isotherm Linear Plots of Cr_2GaC microspheres obtained after furnace annealing using (a) 17-Gauge (b) 18-Gauge (c) 20-Gauge (d) 23-Gauge (e) 26-Gauge (f) 30-Gauge.

(Table 2) and these values are exceptionally high, compared to what has been reported for MAX phases (2.55 – 2.77 m^2/g).[25,36] As discussed later, the microporosity and high surface area are due to the co-presence of the carbonaceous phase in the samples. The observed high surface areas are consistent with the results from the previously reported MAX carbon composites. For example, Zr_2SC carbon composite spheres exhibited BET specific surface area, 626 m^2/g.[37] These Zr_2SC composites were prepared by loading $ZrOCl_2$ solutions into macroporous sulphonated polystyrene-divinylbenzene strong cation exchange resins, which were then heat treated at 1350 °C under a mixed H_2/Ar atmosphere. This differs from the use of the Polymer Type II complex technique that provides higher levels of atomistic homogeneity of the precursors and slightly lower temperatures at 1050 °C that are utilized

for Cr_2GaC composite spheres. The calculated micropore surface areas of the Cr_2GaC microspheres are in the range of 220 – 416 m^2/g, while the external surface areas are in the range of 124 – 226 m^2/g. This is without an apparent trend observed with respect to the synthetic conditions and to the sizes of the microspheres. (Figure S9 showcases relatively similar sorption isotherms for the microwave-annealed microspheres).

All the isotherms can be classified as Type IVa with a distinctive hysteresis, although the gas uptakes (in the absorption branches) are only gradual all the way to the high P/P_o region, showing a lack of dominant mesopore widths. The observed hysteresis loops of Type H2(**a**) (or, less specifically, H2) are known to be given by complex pore structures, with the very broad size distribution of neck widths, in which network effects and pore blocking are important.[38] For all the samples, furthermore, the isotherms exhibit a low-pressure hysteresis at P/P_o less than 0.4. This typically indicates the entrapment of nitrogen molecules within pores of comparable size to the adsorptive or the swelling of the porous structure during the measurement.[39] Since the material is rigid, it is highly unlikely that the latter is the case. Because the hysteresis loops are type H2 and they lack a clear hysteresis loop closure, the adsorption branch was used for all BJH analyses for the samples.[40] The BJH pore size distributions in Figures S10 and S11 indicate the presence of small mesopores. As the pore size decreases, the dV/dlog(D) pore volume increases gradually but shows a sharp increase at around 5 nm, close to the micropore region (< 2 nm). The limitation of the BJH analysis does not allow the detailed analysis of the micropore sizes, but the observed large pore volume in the micropore region is consistent with the fact that 55 to 74 % of the total (BET) surface areas is from the micropore surface areas which were estimated from the t-plot method (Table 2). The smaller than expected BET specific surface area can be rationalized for the 17-gauge spheres due to the lower micropore area and micropore volume, 302 m^2/g and 0.14 cm^3/g, than that of 18-gauge spheres, 413 m^2/g and 0.19 cm^3/g.

Table 2. BET specific surface area, micropore area, external area, and micropore volume of Cr_2GaC microspheres obtained after furnace annealing with varied gauge sizes.

Gauge (mm)/ga	BET SSA (m^2/g)	Micropore Area (m^2/g)	External Area (m^2/g)	Micropore Volume (cm^3/g)

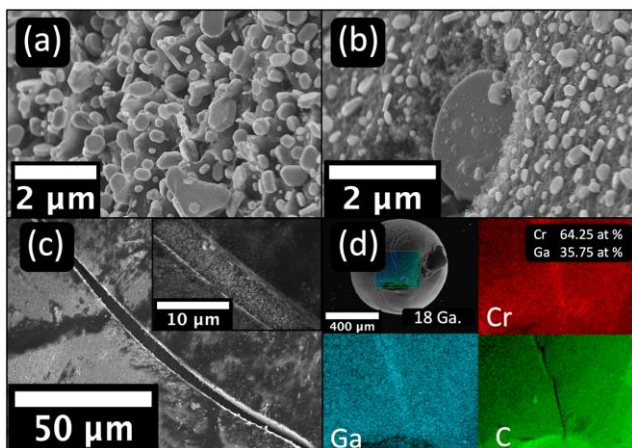| 1.4/17	464	302	162	0.140
1.27/18	616	413	203	0.190
0.91/20	468	345	124	0.159
0.64/23	450	281	169	0.129
0.46/26	396	220	176	0.101
0.31/30	460	300	160	0.138

Figure 3. Exemplary (a)(b)(c) SEM images and (d) EDS mappings of Cr_2GaC microsphere surfaces obtained after furnace annealing (18 ga.)
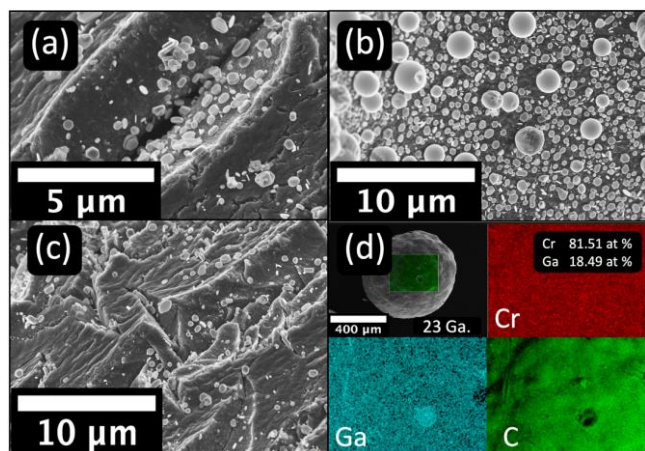

Figure 4. Exemplary (a)(b)(c) SEM images and (d) EDS mapping of Cr_2GaC microsphere surfaces obtained after microwave annealing (23 ga.)

Figures 3 and 4 show exemplary morphology (SEM, a-d) and elemental composition (EDS, d) of the furnace-annealed and microwave-annealed microspheres, respectively. A magnification of the surface for both types of spheres showcase hexagonal and even some spherical plates, which are more prominent decreasing the size of the spheres. (refer to Figure 6-7 for a clearer depiction). The 30 ga. spheres that were reacted via furnace

demonstrated the largest distribution of hexagonal plates on the sphere surface with uniform size (shown in Figure 6, panel (f)). 17 ga. spheres show a noticeable amount of microsphere cracking as spheres of this size cannot handle the outgassing of constituent materials when subjected to microwave heating. EDS measurements for furnace heat treated spheres in Figure 3, panel (d) and Figure S14, panel (a-f) demonstrate a 2-1 ratio of Cr-Ga dispersed homogenously across the spheres of all gauge sizes. Figure S15 shows a deviation of this 2-1 ratio for the microwave spheres because of a tendency of gallium to bleed from samples, as seen in Figure 4 (b). SEM and HR-TEM images of the MAX phase show a very high crystallinity without any pores (Figure 5 (c)). However, a region of strictly microporous carbon in its HR-TEM image (Figure 5(d)) appears as amorphous without apparent lattice fringes. In fact, the observed morphology is quite similar to that of microporous carbon produced from Chitosan in the literature. This is consistent with the gas sorption analysis results of our composite materials.[41] Although the micropores of the carbon phase could not be discerned in
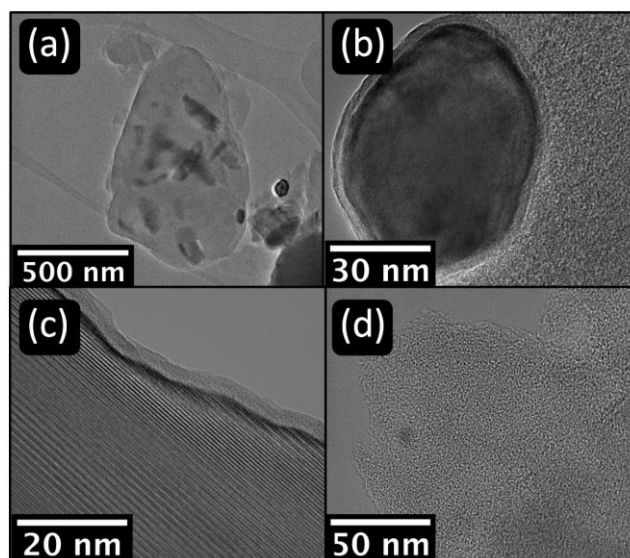

Figure 5. TEM images of Cr_2GaC furnace microspheres: (a) Large particle with crystallite embedded on the surface, (b) crystallite (left-side) and microporous carbon contrast (right-side), (c) MAX phase Cr_2GaC crystallite, (d) region of microporous carbon.

the HR-TEM image, as the disordered, irregularly-shaped micropores are piled upon one another.[42] Figure 5(b)

showcases the contrast between the regions of microporous carbon and MAX phase Cr_2GaC crystallites.
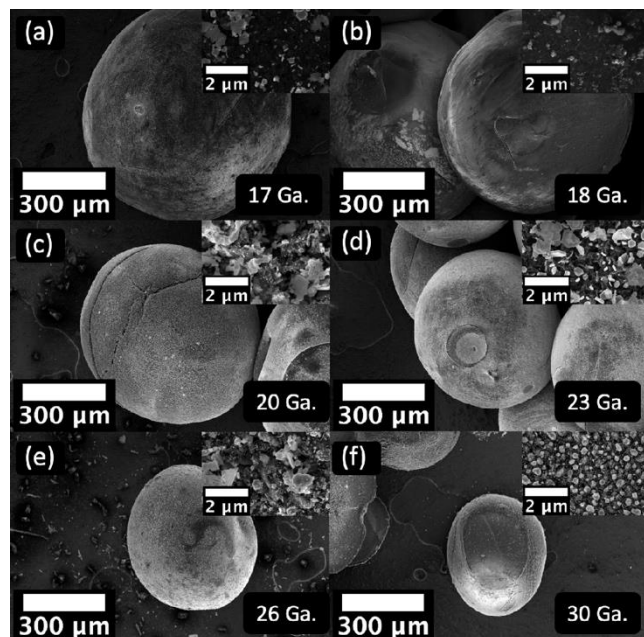

Figure 6. SEM data of Furnace spheres (a) 17-gauge (b) 18-gauge (c) 20-gauge (d) 23-gauge (e) 26-gauge (f) 30-gauge
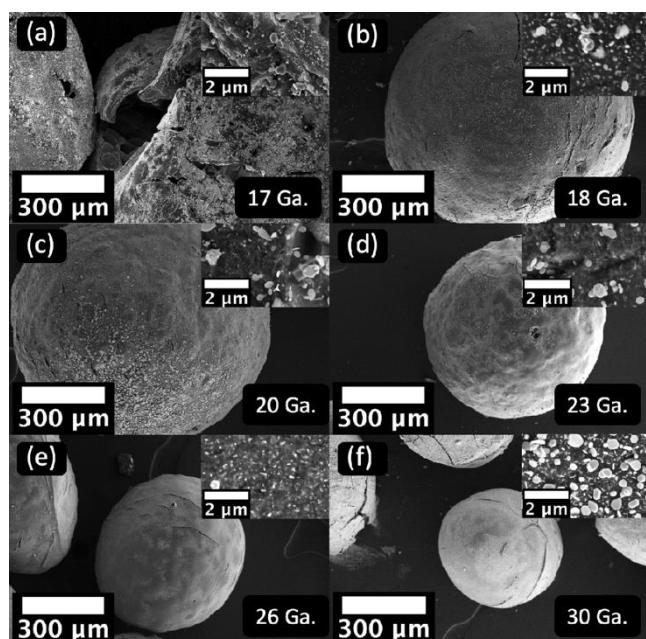

Figure 7. SEM data of Microwave spheres (a) 17-gauge (b) 18-gauge (c) 20-gauge (d) 23-gauge (e) 26-gauge (f) 30-gauge

Conclusions

Sol-gel-based synthesis of MAX carbon composites opens unexplored ways to manipulate the material's morphology and properties. This is demonstrated here by systematically varying the diameter and porosity of carbonaceous Cr_2GaC microspheres. X-ray diffraction and microscopy techniques coupled with element-specific investigations confirm the structure and identity of the MAX phase interspersed throughout the composite spheres and allow for identification of minor side phases. Furthermore, the BET surface area of the Cr_2GaC composite microspheres are discussed. One example of the MAX carbon composite spheres exhibits the highest BET surface area, 616 m^2/g. The shape processability, porosity, and high surface areas were achieved by the choice of natural biopolymer (Chitosan) acting as a gel-building agent during the sol gel-based synthesis as well as the carbon source. This level of tunability of the shape control and properties of MAX phase composites cannot be reached by classical solid-state techniques. This manifests the large potential of sol gel-based methods to synthesize carbide composites that will exhibit advanced properties stemming from the presence of the micropores and the unique MAX phase characteristics, combined in a single material. This study will therefore serve as a foundation for further sol-gel processed products and exploration of their potential application.

Associated Content

Supporting Information

The Supporting Information. "Additional experimental details, including, microwave sphere synthesis, XRD Data, Rietveld Refinements, SEM/EDS analysis, and Microwave BET analysis." (.pdf)

Corresponding Author

*christina.birkel@asu.edu

Author Contributions

J. Sinclair synthesized, measured, and analyzed the samples and wrote the manuscript. J.P. Siebert analyzed the samples and provided research question. D. Ciota performed the gas sorption analysis and pore structure analysis. D.-K. Seo analyzed the gas sorption data and reviewed the manuscript. M. Flores synthesized the samples. C. S. Birkel provided the research question, wrote, and reviewed the manuscript.

ARTICLE

Conflicts of interest

There are no conflicts to declare.

Acknowledgements

ABBREVIATIONS

PXRD, Powder X-Ray Diffraction; BET, Brunner-Emmet-Teller; ILP, Isotherm Linear Plot; BJH, Barret-Joyner-Halenda

References

(1) Von Kudielka, H. Strukturuntersuchungen an Carbosulfiden von Titan Und Zirkon. *Zeitschrift fur Kristallographie - New Crystal Structures* **1960**, *114* (1–6), 447–456. https://doi.org/10.1524/zkri.1960.114.1-6.447.

(2) Barsoum, M. W.; El-Rahy, T. Synthesis and Characterization of a Remarkable Ceramic. 1996. https://doi.org/10.1111/j.1151-2916.1996.tb08018.x.

(3) Radovic, M.; Barsoum, M. W. MAX Phases: Bridging the Gap between Metals and Ceramics. *American Ceramic Society Bulletin* **2013**, *92* (3), 20–27.

(4) Lee, W. E.; Giorgi, E.; Harrison, R.; Maître, A.; Rapaud, O. Ultra-High Temperature Ceramics: Materials for Extreme Environment Applications.

(5) Wang, Z.; Ma, G.; Liu, L.; Wang, L.; Ke, P.; Xue, Q.; Wang, A. High-Performance Cr_2AlC MAX Phase Coatings: Oxidation Mechanisms in the 900–1100°C Temperature Range. *Corros Sci* **2020**, *167* (December 2019). https://doi.org/10.1016/j.corsci.2020.108492.

(6) Zhou, A.; Wang, C. an; Huang, Y. A Possible Mechanism on Synthesis of Ti_3AlC_2. *Materials Science and Engineering A* **2003**, *352* (1–2), 333–339. https://doi.org/10.1016/S0921-5093(02)00937-1.

(7) Wang, X. H.; Zhou, Y. C. Layered Machinable and Electrically Conductive Ti_2AlC and Ti_3AlC_2 Ceramics: A Review. *J Mater Sci Technol* **2010**, *26* (5), 385–416. https://doi.org/10.1016/S1005-0302(10)60064-3.

(8) Lin, Z. J.; Zhuo, M. J.; Zhou, Y. C.; Li, M. S.; Wang, J. Y. Microstructural Characterization of Layered Ternary Ti_2AlC. *Acta Mater* **2006**, *54* (4), 1009–1015. https://doi.org/10.1016/j.actamat.2005.10.028.

(9) Naguib, M.; Kurtoglu, M.; Presser, V.; Lu, J.; Niu, J.; Heon, M.; Hultman, L.; Gogotsi, Y.; Barsoum, M. W. Two-Dimensional Nanocrystals Produced by Exfoliation of Ti_3AlC_2. *Advanced Materials* **2011**, *23* (37), 4248–4253. https://doi.org/10.1002/adma.201102306.

(10) Sokol, M.; Natu, V.; Kota, S.; Barsoum, M. W. On the Chemical Diversity of the MAX Phases. *Trends Chem* **2019**, *1* (2), 210–223. https://doi.org/10.1016/j.trechm.2019.02.016.

(11) Gutzmann, H.; Gärtner, F.; Höche, D.; Blawert, C.; Klassen, T. Cold Spraying of Ti_2AlC MAX-Phase Coatings. *Journal of Thermal Spray Technology* **2013**, *22* (2–3), 406–412. https://doi.org/10.1007/s11666-012-9843-1.

(12) Walter, C.; Martinez, C.; El-Raghy, T.; Schneider, J. M. Towards Large Area MAX Phase Coatings on Steel. *Steel Res Int* **2005**, *76* (2–3), 225–228. https://doi.org/10.1002/srin.200506000.

(13) Xia, Q. X.; Fu, J.; Yun, J. M.; Mane, R. S.; Kim, K. H. High Volumetric Energy Density Annealed-MXene-Nickel Oxide/MXene Asymmetric Supercapacitor. *RSC Adv* **2017**, *7* (18), 11000–11011. https://doi.org/10.1039/c6ra27880a.

(14) Yang, Y.; Xu, Y.; Li, Q.; Zhang, Y.; Zhou, H. Two-Dimensional Carbide/Nitride (MXene) Materials in Thermal Catalysis. **2022**, *3*. https://doi.org/10.1039/d2ta03481f.

(15) Ahmed, B.; Ghazaly, A. El; Rosen, J. I-MXenes for Energy Storage and Catalysis. *Adv Funct Mater* **2020**, *30* (47). https://doi.org/10.1002/adfm.202000894.

(16) Zhu, J.; Ha, E.; Zhao, G.; Zhou, Y.; Huang, D.; Yue, G.; Hu, L.; Sun, N.; Wang, Y.; Lee, L. Y. S.; Xu, C.; Wong, K. Y.; Astruc, D.; Zhao, P. Recent Advance in MXenes: A Promising 2D Material for Catalysis, Sensor and Chemical Adsorption. *Coord Chem Rev* **2017**, *352*, 306–327. https://doi.org/10.1016/j.ccr.2017.09.012.

(17) Mehrabi-kalajahi, S.; Orooji, Y.; Arefi-oskoui, S. Preparasion of Layered V_4AlC_3 MAX Phase for Highly Selective and Efficient Solvent-Free Aerobic Oxidation of Toluene to Benzaldehyde. *Molecular Catalysis* **2022**, *529* (July), 112545. https://doi.org/10.1016/j.mcat.2022.112545.

(18) Wang, B.; Zhou, A.; Liu, F.; Cao, J.; Wang, L.; Hu, Q. Carbon Dioxide Adsorption of Two-Dimensional Carbide MXenes. *Journal of Advanced Ceramics* **2018**, *7* (3), 237–245. https://doi.org/10.1007/s40145-018-0275-3.

(19) Yushin, G.; Hoffman, E. N.; Barsoum, M. W.; Gogotsi, Y.; Howell, C. A.; Sandeman, S. R.; Phillips, G. J.; Lloyd, A. W.; Mikhalovsky, S. V. Mesoporous Carbide-Derived Carbon with Porosity Tuned for Efficient Adsorption of Cytokines. *Biomaterials* **2006**, *27* (34), 5755–5762. https://doi.org/10.1016/j.biomaterials.2006.07.019.

(20) Chirica, I. M.; Mirea, A. G.; Neaţu, Ş.; Florea, M.; Barsoum, M. W.; Neaţu, F. Applications of MAX Phases and MXenes as Catalysts. *J Mater Chem A Mater* **2021**, *9* (35), 19589–19612. https://doi.org/10.1039/d1ta04097a.

(21) Rakhi, R. B.; Ahmed, B.; Hedhili, M. N.; Anjum, D. H.; Alshareef, H. N. Effect of Postetch Annealing Gas Composition on the Structural and Electrochemical Properties of Ti_2CT_x MXene

Electrodes for Supercapacitor Applications. *Chemistry of Materials* **2015**, *27* (15), 5314–5323. https://doi.org/10.1021/acs.chemmater.5b01623.

(22) Liu, Y.; Xie, X.; Liu, Z.; Yu, Q.; Wang, X.; Wang, S.; Jia, Q.; Zhang, Z.; Yang, R.; Ritchie, R. O. Strong and Tough Magnesium-MAX Phase Composites with Nacre-like Lamellar and Brick-and-Mortar Architectures. *Commun Mater* **2023**, *4* (1). https://doi.org/10.1038/s43246-023-00358-3.

(23) Zhang, J.; Chen, K.; Sun, X.; Liu, M.; Hu, X.; He, L.; Huang, Z.; Chai, Z.; Xiao, X.; Song, Y.; Huang, Q. MAX Phase Ceramics/Composites with Complex Shapes. *ACS Appl Mater Interfaces* **2021**, *13* (4), 5645–5651. https://doi.org/10.1021/acsami.0c22289.

(24) Petrus, M.; Wozniak, J.; Cygan, T.; Pawlak, W.; Olszyna, A. Novel Alumina Matrix Composites Reinforced with MAX Phases—Microstructure Analysis and Mechanical Properties. *Materials* **2022**, *15* (19). https://doi.org/10.3390/ma15196909.

(25) Velasco, B.; Gordo, E.; Tsipas, S. A. MAX Phase Ti_2AlC Foams Using a Leachable Space-Holder Material. *J Alloys Compd* **2015**, *646*, 1036–1042. https://doi.org/10.1016/j.jallcom.2015.05.235.

(26) Danks, A. E.; Hall, S. R.; Schnepp, Z. The Evolution of "Sol-Gel" Chemistry as a Technique for Materials Synthesis. *Mater Horiz* **2016**, *3* (2), 91–112. https://doi.org/10.1039/c5mh00260e.

(27) Siebert, J. P.; Bischoff, L.; Lepple, M.; Zintler, A.; Molina-Luna, L.; Wiedwald, U.; Birkel, C. S. Sol-Gel Based Synthesis and Enhanced Processability of MAX Phase Cr_2GaC. *J Mater Chem C Mater* **2019**, *7* (20), 6034–6040. https://doi.org/10.1039/c9tc01416k.

(28) Siebert, J. P.; Patarakun, K.; Birkel, C. S. Mechanistic Insights into the Nonconventional Sol-Gel Synthesis of MAX Phase M_2GeC (M = V,

Cr). *Inorg Chem* **2022**, *61* (3), 1603–1610. https://doi.org/10.1021/acs.inorgchem.1c03415.

(29)   Siebert, J. P.; Mallett, S.; Juelsholt, M.; Pazniak, H.; Wiedwald, U.; Page, K.; Birkel, C. S. Structure Determination and Magnetic Properties of the Mn-Doped MAX Phase Cr_2GaC. *Mater Chem Front* **2021**, *5* (16), 6082–6091. https://doi.org/10.1039/d1qm00454a.

(30)   Kubitza, N.; Reitz, A.; Zieschang, A. M.; Pazniak, H.; Albert, B.; Kalha, C.; Schlueter, C.; Regoutz, A.; Wiedwald, U.; Birkel, C. S. From MAX Phase Carbides to Nitrides: Synthesis of V_2GaC, V_2GaN, and the Carbonitride $V_2GaC_{1-x}N_x$. *Inorg Chem* **2022**, *61* (28), 10634–10641. https://doi.org/10.1021/acs.inorgchem.2c00200.

(31)   Sinclair, J.; Siebert, J. P.; Juelsholt, M.; Shen, C.; Zhang, H.; Birkel, C. S. Sol Gel-Based Synthesis of the Phosphorus-Containing MAX Phase V_2PC. *Inorg Chem* **2022**, *61* (43), 16976–16980. https://doi.org/10.1021/acs.inorgchem.2c02880.

(32)   Siebert, J. P.; Flores, M.; Birkel, C. S. Shape Control of MAX Phases by Biopolymer Sol–Gel Synthesis: Cr_2GaC Thick Films, Microspheres, and Hollow Microspheres . *ACS Organic & Inorganic Au* **2022**, *2* (1), 59–65. https://doi.org/10.1021/acsorginorgau.1c00022.

(33)   Siebert, J. P.; Hajra, D.; Tongay, S.; Birkel, C. S. The Synthesis and Electrical Transport Properties of Carbon/Cr_2GaC MAX Phase Composite Microwires. *Nanoscale* **2022**, *14* (3), 744–751. https://doi.org/10.1039/d1nr06780j.

(34)   Coelho, A. A. TOPAS and TOPAS-Academic: An Optimization Program Integrating Computer Algebra and Crystallographic Objects Written in C++: An. *J Appl Crystallogr* **2018**, *51* (1), 210–

218. https://doi.org/10.1107/S1600576718000183.

(35)   Brunauer, S.; Emmett, P. H.; Teller, E. *Adsorption of Gases in Multimolecular Layers*; 1938. https://pubs.acs.org/sharingguidelines.

(36)   Piechowiak, M. A.; Henon, J.; Durand-Panteix, O.; Etchegoyen, G.; Coudert, V.; Marchet, P.; Rossignol, F. Growth of Dense Ti_3SiC_2 MAX Phase Films Elaborated at Room Temperature by Aerosol Deposition Method. *J Eur Ceram Soc* **2014**, *34* (5), 1063–1072. https://doi.org/10.1016/j.jeurceramsoc.2013.11.019.

(37)   Scales, N.; Chen, J.; Aughterson, R. D.; Karatchevtseva, I.; Stopic, A.; Lumpkin, G. R.; Luca, V. Porous Zr_2SC-Carbon Composite Microspheres: Possible Radiation Tolerant Sorbents and Transmutation Hosts for Technetium-99. *Microporous and Mesoporous Materials* **2018**, *259*, 67–78. https://doi.org/10.1016/j.micromeso.2017.09.033.

(38)   Thommes, M.; Kaneko, K.; Neimark, A. V.; Olivier, J. P.; Rodriguez-Reinoso, F.; Rouquerol, J.; Sing, K. S. W. Physisorption of Gases, with Special Reference to the Evaluation of Surface Area and Pore Size Distribution (IUPAC Technical Report). *Pure and Applied Chemistry* **2015**, *87* (9–10), 1051–1069. https://doi.org/10.1515/pac-2014-1117.

(39)   Lowell, S.; Shields J.E.; Thomas M. A.; Thommes M. *Characterization of Porous Solids and Powders: Surface Area, Pore Size and Density*; 2004. https://doi.org/10.1007/978-1-4020-2303-3.

(40)   Volosin, A. M.; Chen, S.; Seo, D. K. High-Surface Area Mesoporous Carbons from Gel Templating and Inorganic-Organic Hybrid Gel Formation. *J Solid State Chem* **2020**, *281*. https://doi.org/10.1016/j.jssc.2019.121040.

(41)   Fan, X.; Zhang, L.; Zhang, G.; Shu, Z.; Shi, J. Chitosan Derived Nitrogen-Doped Microporous Carbons for High Performance CO_2 Capture. *Carbon N Y* **2013**, *61*, 423–430. https://doi.org/10.1016/j.carbon.2013.05.026.

(42)   Oshida, K. Image Analysis. In *Materials Science and Engineering of Carbon: Characterization*; Elsevier, 2016; pp 95–123. https://doi.org/10.1016/B978-0-12-805256-3.00006-4.